EXPLORING POLARIMETRIC SIGNALS INDUCED BY COMPACT LENSING OBJECTS TOWARD THE GALACTIC CENTER

MARSIDA LAZE[1], LINDITA HAMOLLI[2], MIMOZA HAFIZI[2]

[1]Department of Physics, Faculty of Natural Sciences,

University of Elbasan "Aleksander Xhuvani", Elbasan, Albania

[2]Department of Physics, Faculty of Natural Sciences,

University of Tirana, Tirana, Albania

e-mail: marsida.laze@uniel.edu.al

Abstract

Gravitational microlensing phenomenon occurs when compact objects pass in front of background sources, bending and magnifying their light. However, parameters derived from standard photometric microlensing light curves are affected by strong degeneracies, preventing a unique determination of the lens properties. These degeneracies can be partially broken by measuring second order effects, such as parallax and finite-source effects, as well as through astrometric observations. Polarimetric measurements during microlensing events provide an additional and promising approach. In particular, light from stars with extended atmospheres can become polarized through scattering processes within their circumstellar envelopes. Microlensing effect can break spherical symmetry, resulting in a detectable polarization signal, particularly for stars with extended atmosphere. Polarimetric observations can constrain the Einstein angular radius, the direction of the lens trajectory, and the transverse velocity. Considering the future microlensing observations towards the Galactic bulge by the Nancy Grace Roman Space Telescope, we explore possibility of detection of polarization signal by FORS2 at the Very Large Telescope (VLT). We find that the lens with mass in range $[10^{-3}, 10]\ M_{\odot}$ *and distances up to 5kpc can produce a measurable polarization signal and their detection probability is* 1.6%*. We emphasize that these events are important because, beyond the constraints on the lens parameters that can be found by second-order effects, they also enable the determination of the direction of the lens movement, which is especially important when the lenses are dark objects.*

Key words: *microlensing, polarization, extended envelope.*

Përmbledhje

Fenomeni i mikropërthyerjes gravitacionale ndodh kur objektet kompakte kalojnë përpara burimeve në sfond, duke përkulur dhe zmadhur dritën e tyre. Megjithatë, parametrat që marrim nga kurbat fotometrike standarde të mikropërthyerjes vuajnë nga degjenerime të forta, të cilat pengojnë përcaktimin në mënyrë të vetme të vetive të lentes. Këto degjenerime mund të hiqen pjesërisht përmes matjes së efekteve të rendit të dytë, si paralaksi dhe efektet e burimit me madhësi të fundme, si edhe përmes vëzhgimeve astrometrike. Matjet e sinjalit polarimetrik gjatë ngjarjeve të mikropërthyerjes janë gjithashtu një mundësi premtuese. Në veçanti, drita nga yjet me atmosfera të zgjeruara mund të polarizohet përmes proceseve të shpërhapjes brenda mbështjelljeve të tyre rrethore. Efekti i mikropërthyerjes thyen simetrinë sferike të burimit, duke rezultuar në një sinjal polarizimi të varur nga koha dhe potencialisht të detektueshëm, sidomos për yjet me atmosferë të zgjeruar. Vëzhgimet polarimetrike mund të kufizojnë parametra kyç të lentes, si rrezja këndore e Ajnshtajnit, drejtimi i trajektores së lentes dhe shpejtësia transversal. Duke marrë parasysh vrojtimet e ardhshme të mikrothyerjes drejt bulbit galaktik nga Nancy Grace Roman Space Telescope, ne eksplorojmë mundësinë e zbulimit të sinjalit të polarizimit me instrumentin FORS2 në Very Large Telescope (VLT). Vleresojme se lentet me masa $[10^{-3}, 10]\, M_{\odot}$ *dhe distancat deri në 5 kpc që janë në gjendje të prodhojnë një sinjal polarizimi të, me një probabilitet zbulimi prej* 1.6%*. Theksojmë se këto ngjarje janë të rëndësishme sepse, përtej percaktimeve mbi parametrat e lentes që gjenden nga efektet të rendit të dytë, ato gjithashtu mundësojnë përcaktimin e drejtimit të lëvizjes së lentes, gjë që është veçanërisht e rëndësishme kur lentet janë objekte të errëta.*

Fjalë kyçe: *mikropërthyerje, polarizim, atmosfera e zgjeruar.*

Introduction

Gravitational microlensing is a powerful astrophysical phenomenon which occurs when a massive body such as a star, planet, or compact dark matter object approaches the line of sight towards a distant background source. The gravitational field of the transiting object (lens) bends the light of the source star, forming two images, which are very close to each other. With today's telescopes, these are not resolved, but a rise and then a fall in the luminosity of the source can be observed (Einstein et al., 1936).

Since this method does not rely on the light from the lens, it is used by several projects for the detection of dark matter. Microlensing surveys such as MACHO (Alcock et al., 2000), EROS (Tisserand et al., 2007), OGLE (Wyrzykowski et al., 2011), and MOA (Bond et al., 2001) have put useful bounds on the contribution of compact objects to dark matter. It has also emerged as a crucial method for detecting extrasolar planets, particularly those with large orbital separations or low masses, which are hard to identify via radial velocity or transit techniques (Sumi et al., 2011; Gaudi et al., 2012). Moreover, the increased cadence of microlensing observations has made it possible to detect lensing objects with masses down to the order of Earth, providing a direct way to probe and constrain the components of dark matter over a wide range of masses (Niikura et al., 2019). Despite its wide applicability, a standard microlensing light curve provides only limited physical information. Among the measurable quantities, only the Einstein timescale carries information about the lens, so its parameters cannot be uniquely determined (Dominik et al., 2009; Sajadian et al., 2023). One approach to partially resolve this degeneracy is to consider second-order effects such as parallax, astrometric shifts, or finite-source effects (Hamolli et al., 2019).

Moreover, lens parameters can also be constrained through polarimetric observations of the microlensing events. Different regions of the stellar disc are magnified unevenly, inducing a small net polarization signal (Simmons et al., 1995a, b). This effect is particularly pronounced in stars with extended circumstellar envelopes. For instance, cool red giant branch (RGB) stars surrounded by dusty winds can produce polarization signals of up to $\sim$10% due to scattering by dust grains (Ingrosso et al., 2014). Khalouei et al. (2021) demonstrated that polarimetric microlensing can be used not only to reduce lens parameter degeneracies but also to constrain properties of the source atmosphere, such as the scattering optical depth and the inner radius of the circumstellar envelope.

In this work, we explore the possibility of detecting polarimetric signals in microlensing events towards the Galactic bulge. For this purpose, we consider the planned photometric observations with the Nancy Grace Roman Space Telescope, as well as follow-up polarimetric observations with FORS2 at the VLT. The Nancy Grace Roman Space Telescope, developed by NASA, is an infrared observatory scheduled for launch in May 2027 and will operate at the second Lagrange point (L2). Its main scientific aim is to explore dark energy through several observational techniques. Equipped with the Wide Field

Instrument (WFI), the telescope provides a 0.281 deg^2 field of view and will survey approximately 2,000 deg^2 in the near-infrared during its five-year mission, achieving an angular resolution of $0.1''$ (Spergel et al., 2015). Roman will carry out a dedicated microlensing survey of the Galactic bulge[1], monitoring approximately seven fields with a total area of $\sim 2\ deg^2$, centered at ($l = 0.8°, b = -1.4°$), with photometric precision at the 1% level and a cadence of about 15 minutes. FORS2 is a spectrograph designed for the Very Large Telescope (VLT), providing both direct imaging and spectroscopy capabilities for astronomical observations. It operates in the visual and near ultraviolet range, covering wavelengths from 330 nm to 1100 nm. The optimum value of precision for the FORS2[2] polarimeter is 0.1 %.

This paper is structured as follows. We continue with the basics of photometric microlensing, then introduce the theoretical framework for polarization signals. Next, we present our simulations and results, and finally conclude with the main findings.

Amplification in microlensing events

A microlensing event is characterized by three key parameters: the time of maximum amplification (t_0), which marks the peak of the event; the Einstein timescale ($t_E = R_E/V_T$), representing the time it takes the lens to cross the Einstein radius R_E, moving with the relative transverse velocity V_T. The Einstein radius is given by:

$$R_E = \sqrt{\frac{4GM_L}{c^2}\left(\frac{1}{D_L} - \frac{1}{D_S}\right)}, \quad (1)$$

where G is the gravitational constant, M_L is the lens mass, D_L and D_S are the distances to the lens and source, respectively. The third parameter is the impact parameter (u_0), the minimum value of the separation $u(t)$ between the lens and the line of sight in units of R_E. It varies by time,

$$u(t) = \sqrt{u_0^2 + \left[\frac{t-t_0}{t_E}\right]^2}. \quad (2)$$

[1] https://roman.gsfc.nasa.gov/science/Galactic_Bulge_Time_Domain_Survey.html
[2] https://www.eso.org/public/teles-instr/paranal-observatory/vlt/

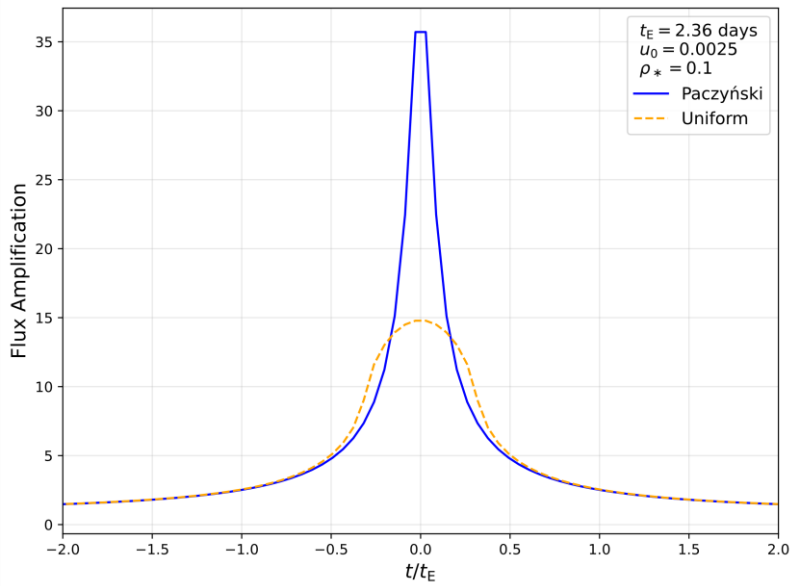

Figure 1: Amplification curve of a microlensing event. The solid blue line represents the standard point-source model, while the dashed orange line shows the effect of a uniformly bright finite source with a projected radius in the lens plane $\rho_* = 0.1$.

In the standard point-source approximation, the magnification of a microlensing event is described by the Paczyński profile (Paczyński et al., 1986)

$$A = \frac{u^2+2}{u\sqrt{u^2+4}}. \quad (3)$$

This results in a symmetric light curve that reaches its maximum when the lens is closest to the source. Photometric microlensing light curves primarily constrain the t_E, a quantity that entangles the lens mass, distance, and transverse velocity, leading to strong degeneracies. These degeneracies can be partially broken by including second-order effects, such as the finite-source effects.

When the angular size of the source is non negligible, the point source approximation fails, and the observed amplification must be averaged over the stellar disc. In the case of a uniform source, the observed amplification must be averaged over the stellar disc (see Hamolli et al., 2015 for details).

The finite size of the source leads to a smoothing of the magnification peak compared to the point-source case (see Figure 1). In such finite-source configurations, the lens produces an uneven magnification across the stellar disc and polarimetric observation can lead to a net polarization signal (Ingrosso et al., 2012).

Polarization in microlensing events

It is known that the light from a spherically symmetric star is inherently unpolarized, but as a lens transits a source star with an extended atmosphere or circumstellar envelope, it magnifies different regions unequally. This selective amplification creates an asymmetry in the scattered light, generating a net polarization signal.

Simmons et al., (2002) investigated the polarization signal in microlensing events involving source stars surrounded by a spherically symmetric, optically thin circular envelope. In this model, the envelope is characterized by a radial density profile $n = n_0(\frac{R_h}{r})^{\beta}$ which may also include a central cavity with radius R_h. Microlensing introduces differential magnification across the source and its envelope, breaking the inherent symmetry and producing a net polarization signal.

The resulting polarization signal is quantified using the Stokes parameters: I, Q, U and V, where I is the total intensity, Q is the difference in intensity measured in two perpendicular directions, x and y, U is the difference in intensity measured in two perpendicular directions at 45° to the x and y axes and V measures any circular polarization (Tinbergen et al., 2005). The observable fractional polarization and its position angle are given in terms of the integrated Stokes flux vector $\boldsymbol{F} = (F_I, F_Q, F_U, F_V)^T$ by:

$$P = \frac{\sqrt{F_Q^2+F_U^2+F_V^2}}{F_I},\ \psi = \frac{1}{2} arctan \frac{F_U}{F_Q}. \quad (4)$$

The observed Stokes fluxes are given by integrals over the source profile: for each Stokes component:

$$\boldsymbol{F} = \frac{1}{D_S^2}\int_{source} A(p,\alpha;p_S,\alpha_S) I(p,\alpha) p dp d\alpha, \quad (5)$$

where (p_S, α_S) are the polar coordinates of the source center in the lens plane. $\boldsymbol{I} = (I, Q, U, V)^T$ expresses the local Stokes intensities of each source element located in polar coordinates (p, α), given by (Simmons et al., 2002):

$$\boldsymbol{I}(p,\alpha) = \boldsymbol{I}_0(p) + \frac{3}{16} I_*(\beta-1)\left(\frac{R_h}{p}\right)^{\beta-1}\left(\frac{\rho_*}{p}\right)^2 \tau_{sc} \times g_0(p) \begin{pmatrix} G_I \\ G_P \cos 2\alpha \\ -G_P \sin 2\alpha \\ 0 \end{pmatrix}, \quad (6)$$

where

$$\boldsymbol{I}_0(p) = \begin{cases} (I_*, 0, 0, 0)^T & (p < \rho_*) \\ 0 & (p \geq \rho_*) \end{cases}.$$

Due to spherical symmetry, the amplified flux and polarization are independent of the angle α_S, thus, we can rotate the source-plane variables to (p, α'), where $\alpha' = \alpha - \alpha_S$ (see Fig. 1 at Simmons et al. 2002 for details).

The total observed Stokes flux is then given by

$$\frac{\boldsymbol{F}}{F_*} = \frac{\boldsymbol{F_0}}{F_*} + \frac{3(\beta-1)}{16\pi} R_h^{\beta-1} \tau_{sc} \int_0^\infty p dp \int_0^{2\pi} A(p,\alpha') d\alpha' \times \frac{g_0(p)}{p^{\beta+1}} \begin{pmatrix} G_I(p) \\ G_P(p)\cos(2\alpha')\cos(2\alpha_S) \\ -G_{P(p)}\cos(2\alpha')\sin(2\alpha_S) \\ 0 \end{pmatrix}, \quad (7)$$

where

$$\frac{\boldsymbol{F_0}}{F_*} = \frac{1}{\pi\rho_*^2} \int_0^{2\pi} d\alpha' \int_0^{\rho_*} \frac{\boldsymbol{I_0}}{I_*} A\,(p,\alpha')\, p\, dp, \quad (8)$$

is the lensed stellar flux, with $F_* = \pi I_* \theta_*^2$ and the functions $G_I(p)$ and $G_P(p)$ are defined by eq. 19-21 in Simmons et al., (2002). The contribution of the stellar disc and the envelope to the amplified flux and polarization can be expressed through suitable integrals over the source profile. Using this formalism, the Stokes parameters can be conveniently written as:

$$\frac{\boldsymbol{F}}{F_*} = \begin{bmatrix} H_*(p_S) + \tau_{sc} H_I(p_S) \\ \tau_{sc} H_p(p_S)\cos(2\phi) \\ -\tau_{sc} H_p(p_S)\sin(2\phi) \\ 0 \end{bmatrix}. \quad (9)$$

The total flux amplification by lensing is calculated by:

$$M(p_S) = H_*(p_S) + \tau_{sc} H_I(p_S), \quad (10)$$

and the signal polarization by:

$$P(p_S) = \frac{\tau_{sc} H_p(p_S)}{H_*(p_S) + \tau_{sc} H_I(p_S)}. \quad (11)$$

Furthermore, by polarimetric measurements the polarization angle can be defined:

$$\Psi = \pi - \tan^{-1}\left[\frac{\theta_0}{\mu_{rel}(t-t_0)}\right]. \quad (12)$$

During a microlensing event, at closest approach, the direction of the polarization is parallel to the direction of travel of the lens. By analyzing the rate of change of the polarization angle, observers can determine the direction and magnitude of the relative proper motion of the lens μ_{rel}. This is achieved by measuring the timescale of the angle's variation, $t_\Psi = \theta_0/\mu_{rel}$, where θ_0 is the angular position between the lens and the source at time t_0, which can be inferred from photometric data (see Simmons et al., 2002 for details).

When the source star is surrounded by a circumstellar envelope, the observed flux consists of both the direct stellar flux and the flux scattered by the envelope. In Figure 2, the total amplification including polarization effects is represented by the dashed orange curve, while the amplification without an envelope is shown by the solid blue curve. In certain cases, the difference between these curves exceeds the photometric error of the instrument, indicating that the envelope's contribution cannot be neglected.

The inner circumstellar radius of the envelope, R_h is defined by

$$R_h = 0.45\left(\frac{T_{eff}}{T_h}\right)^{2.5} R_*, \quad (13)$$

where $T_h = 1400$ is the temperature at which dust grains begin to form (Ingrosso et al., 2015).

The scattering optical depth τ_{sc}, is a function of the mass-loss rate, terminal dust velocity v_∞ , and R_h (Ignace et al., 2008). It is given by:

$$\tau_{sc} = 2\times10^{-3}\eta\kappa\left(\frac{\dot{M}}{10^{-9}M_\odot yr^{-1}}\right)\left(\frac{30kms^{-1}}{v_\infty}\right)\left(\frac{24R_\odot}{R_h}\right). \quad (14)$$

Here, η denotes the dust-to-gas mass density ratio, $\kappa \approx 200\, cm^2\, g^{-1}$ is the dust opacity for wavelengths longer than 5500 Å (Origlia et al., 2002), v_∞ is the terminal velocity of the dusty stellar wind, given by:

$$v_\infty = 14\left(\frac{L_*}{1000L_\odot}\right)^{0.3}\left(\frac{\varrho}{200}\right)^{-0.5}\left(\frac{km}{s}\right), \quad (15)$$

and the mass loss of the stars, is given by Reimers (1975):

$$\dot{M} = 4\xi\times10^{-13}\frac{(L_*/L_\odot)}{\left(\frac{g_*}{g_\odot}\right)\left(\frac{R_*}{R_\odot}\right)}(M_\odot yr^{-1}). \quad (16)$$

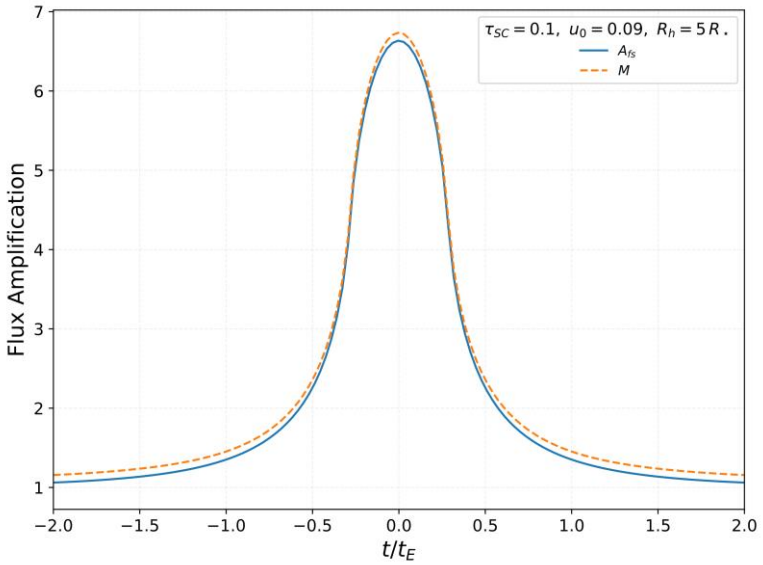

Figure 2. The time variation of the total amplification including polarization effects from the envelope is shown with a dashed orange line, while the amplification without these effects is presented by a solid blue line. The parameters used are: $\tau_{SC} = 0.1$, $u_0 = 0.09$ and $R_h = 5R_*$.

Ingrosso et al., (2012) conclude that the polarization signal is significantly stronger in cool red giant branch (RGB) stars. These stars possess large, low-gravity atmospheres with effective temperatures ranging from 3500 K to 5000 K, making them both cool and convective. Due to their extended size and low surface gravity, RGB stars exhibit high mass-loss rates and tend to develop dusty or ionized envelopes with optical depths optimal for single scattering.

During polarimetric observations, two distinct profiles can be observed. *Transit events***:** In this case, the lens trajectory crosses the stellar disc and its inner scattering envelope. The resulting polarization light curve exhibits a characteristic double-peaked structure, with maxima occurring when the lens passes near the inner radius R_h. The time interval between these two peaks can be calculated by,

$$\delta t = 2t_E\sqrt{(\frac{\bar{R}_h}{0.75})^2 - u_0^2}, \tag{17}$$

where $\bar{R}_h = (R_h/R_E)(D_L/D_S)$). *Bypass events*: In this scenario, the lens does not overlap the source disc. Instead, a single, broader polarization peak is produced as the lens passes closest to the source center, and the overall polarization amplitude is lower.

Simulations and results

Our goal is to investigate the polarization signal in microlensing events produced by dark objects along the line of sight to the Galactic Center. The strength of this signal depends on both the source and lens parameters. Focusing on primordial black holes (PBHs), we first assess the impact of lens mass and distance by performing numerical calculations over a broad range of masses $[10^{-14} - 10^5]M_\odot$ (Sureda et al., 2021) and distances from 0 to 8.5 kpc. Specifically, by considering a stellar radius $R_* = 20R_\odot$, an inner envelope radius $\mathrm{R_h} = 9\mathrm{R_*}$ (the mean values of generated star sample, look below), a scattering optical depth of $\tau_{SC} = 0.1$ and $D_L = 4\ kpc$, we find that lens masses in the range $[10^{-3} - 10]M_\odot$, are likely to produce detectable polarization signals above the FORS2 threshold of 0.1%. In Figure 3, the top panel shows the polarization signal for the transit regime, while the bottom panel shows the bypass regime. In the case of the *Transit Regime*, for lens masses $M_L \leq 10^{-3}M_\odot$, the polarization is negligible, falling below the detection threshold. As the lens mass increases within the range $[10^{-3} - 10]M_\odot$, the polarization signal grows because increasing the lens mass alone increases the Einstein radius, which reduces the impact parameter. For *Bypass Regime*, however, detectable polarization signals are obtained only for lens masses $M_L \geq 10^{-2}M_\odot$. In both regimes, for lens masses $M_L \geq 10M_\odot$, the polarization saturates and no longer increases significantly, because the Einstein radius exceeds the size of the dust-forming region of the circumstellar envelope. For such cases, the lens magnifies the entire dust scattering region, so further increases in lens mass do not enhance the polarization asymmetry.

We further investigate the dependence of the polarization signal on lens distance for two fixed lens masses, corresponding to the boundaries of the mass range that yields detectable polarimetric signals, as illustrated in Figures 4 and 5. Figure 4 presents transit events, while Figure 5 presents bypass events. In each figure, the polarization signal is shown for different lens distances. The low-mass case corresponds to $M_L = 10^{-3}M_\odot$ for transit events and to $M_L = 10^{-2}M_\odot$ for bypass events, representing the minimum

lens mass that produce detectable polarization in the two regimes. The high-mass case corresponds to $M_L = 10M_\odot$ in both figures.

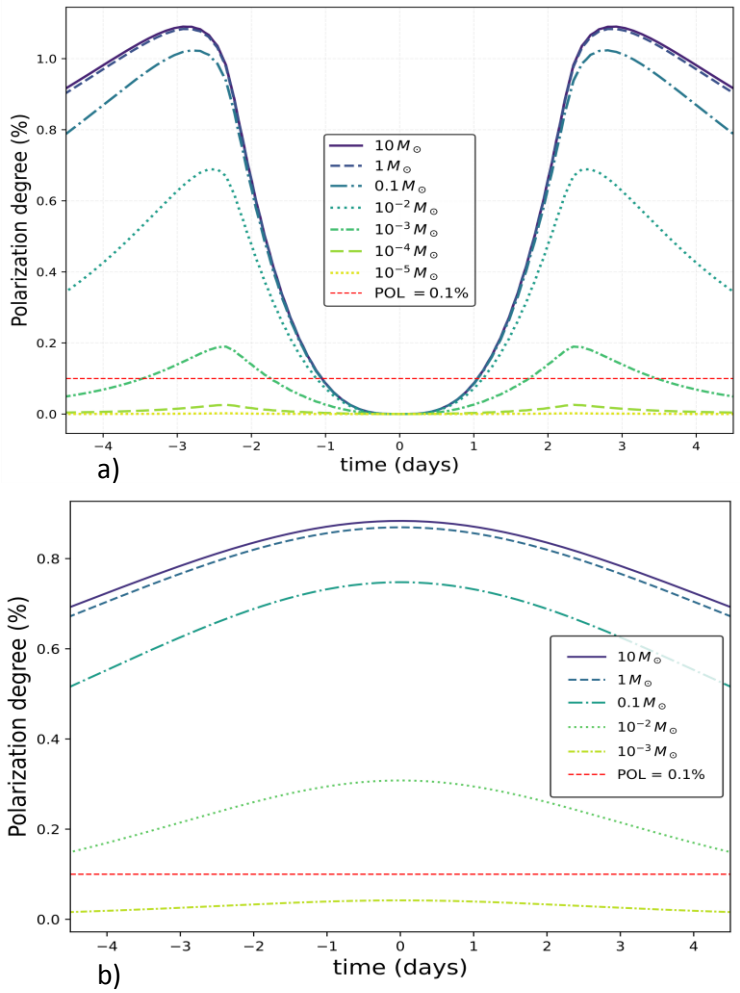

Figure 3. Time evolution of polarization signal during microlensing transit events (a) and bypass events (b). Each curve is for a different value of M_L and a fixed distance of $D_L = 4\ kpc$ from the observer. The dashed red lines show the polarization sensitivity threshold of the FORS2 polarimeter at the VLT. For the same lens mass, bypass events reach lower peak polarization values than transit events

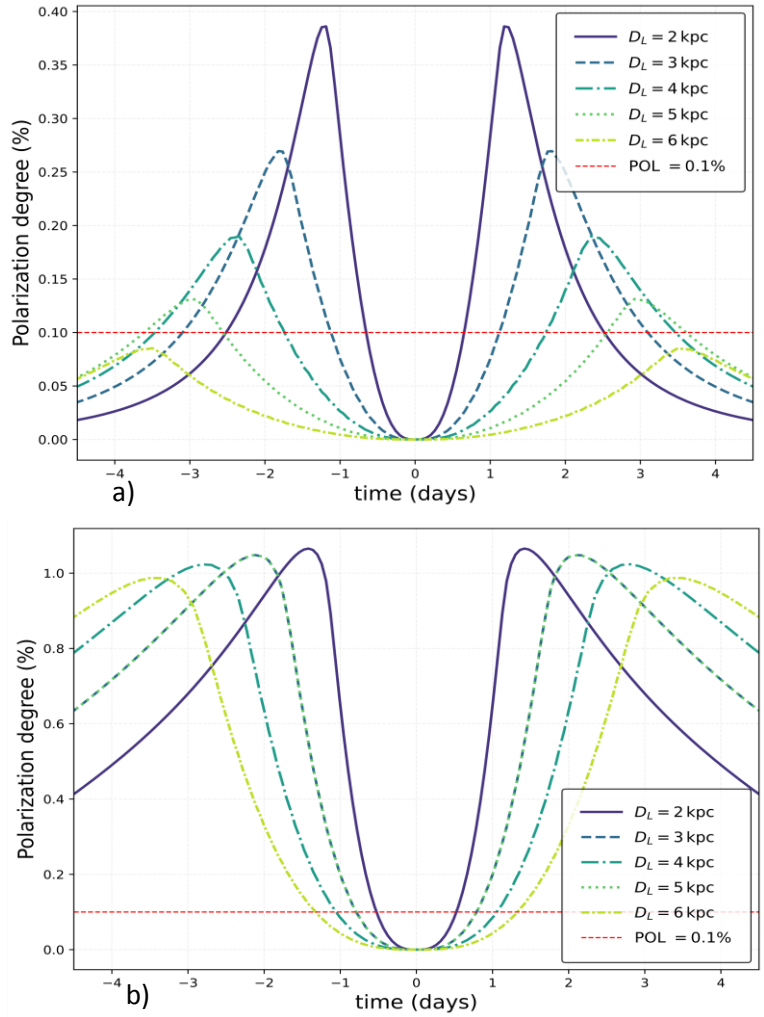

Figure 4. Time evolution of the polarization signal for microlensing transit events. a) polarization curves for different lens distances at a fixed mass of $10^{-3}M_{\odot}$. b) the corresponding curves for a $10M_{\odot}$ lens. The dashed red line shows the polarization sensitivity threshold of FORS2/VLT.

For the low-mass limit in both the transit and bypass regimes, increasing the lens distance leads to a systematic decrease in the polarization amplitude. This behavior reflects the reduced lensing efficiency as the lens approaches the source, which weakens the differential magnification across the dust-scattering region.

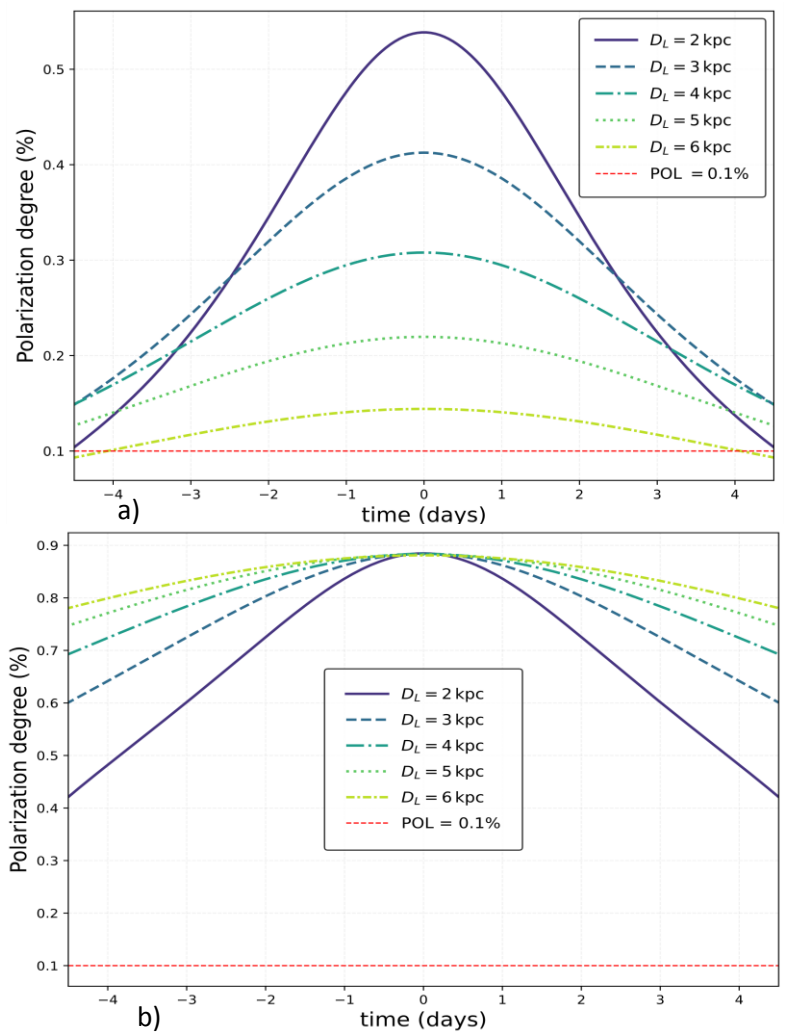

Figure 5. Polarization curves of microlensing bypass events for different lens distances at a fixed mass of $10^{-2}M_{\odot}$ (a) and a mass of $10M_{\odot}$ (b). The dashed red line shows the polarization sensitivity threshold of FORS2/VLT.

In contrast, for the high-mass limit, the maximum polarization remains approximately constant with increasing distance. In this case, the Einstein radius is already larger than the dust-forming region of the envelope, so changes in lens distance mainly affect the event timescale, resulting in broader polarization profiles without significantly altering the peak polarization.

We note that the results shown in these figures are obtained under a specific set of assumptions for the stellar and envelope parameters, and variations in these properties may quantitatively affect the polarization amplitude, although the qualitative trends remain unchanged.

Monte Carlo method

To investigate the detectability of polarization signatures in microlensing events expected to be observed by the Roman telescope, we focus on the line of sight defined by its galactic coordinates ($b = -1.4°, l = 0.8°$). The sources are assumed to lie in the Galactic bulge, while the primordial black holes (PBHs) are distributed along the line of sight. Their mass distributions are modeled as follows:

Source mass distribution: The sources are taken to reside in the Galactic bulge, with a mass density distribution given by Hafizi et al. (2004)

$$\rho_b = \frac{M_b}{8\pi abc} exp\left(-\frac{s^2}{2}\right), \quad (18)$$

where $s^4 = (x^2/a^2 + y^2/b^2)^2$, the scale length values are $a = 1.49kpc$, $b = 0.58kpc$, $c = 0.40kpc$ and the bulge mass is $M_b = 2 \times 10^{10} M_\odot$.

PBH mass distribution: These objects are assumed to constitute a fraction f of the dark matter in the Galactic halo, with a mass density profile given by Green et al. (2017):

$$\rho_{DM}(r) = \rho_0 \frac{r_c^2 + r_0^2}{r_c^2 + r^2}, \quad (19)$$

where r is the galactocentric radius, $\rho_0 = 0.0079 M_\odot pc^{-1}$ is the local dark matter density, $r_c \approx 5.6\ kpc$ is the halo dark matter core radius and $r_0 \approx 8.5 kpc$ is the galactocentric distance of the Sun.

We employ the Monte Carlo method to extract the source and lens parameters as described below:

- To obtain the envelope parameters necessary for calculating the polarization signal, we use the IAC-STAR online synthetic star population generator (http://iac-star.iac.es/cmd/) to simulate $log\ L$, $log\ g$, $logT_{eff}$, and metallicity Z for 10,000 sources. This generation is based on the stellar evolution models of Bertelli et al., (1994) and the bolometric correction tables from Lejeune et al., (1997). Next, we apply the HIT or MISS algorithm to select a representative sample of 1,000 sources. For each selected source, we estimate the envelope optical depth using equation (14).

- To simulate the source distance, D_S, we use the spatial distribution of source stars given by eq. (18).

- For the distance of the lens, we use the halo distribution given by eq. (19).

- The relative transverse velocity is derived from the individual velocities of the source, lens, and observer, each modeled using Maxwellian distributions. Specifically, the PBH lens (halo) is assigned a one-dimensional velocity dispersion of $\sigma_L = 210\ km$, the stars in the bulge have $\sigma_S = 156\ km/s$, and the Sun, representing the observer in the thin disk, has $\sigma_\odot = 30\ km/$s (for details, see Hamolli et al., 2021)

- We consider lens masses that produce polarization signals detectable by FORS2 over a wide range, from $[10^{-5} - 10]M_\odot$, sampling them uniformly on a logarithmic scale.

- Given that our analysis focuses on the Roman Space Telescope, which offers photometric precision better than 1%, we adopt a detection threshold of $A_{th} = 1.01$, corresponding to a maximum impact parameter of $u_0 = 3.5$. To ensure broad coverage of potential microlensing configurations, we generate u_0 values uniformly distributed over the range $[0, 3.5]$.

To match the observing cadences of both the Roman telescope (15 minutes) and the FORS2 instrument (18 minutes) used for polarimetric follow-up, we adopt a cadence of 20 minutes, suitable for both photometric and polarimetric measurements.

For each event, we calculate the amplification under two configurations: (i) including finite-source effects, (ii) including the circumstellar envelope, and the resulting polarization signal. We also quantify the number of data points where the polarization signal exceeds 0.001. Events with more than five such points are classified as exhibiting detectable polarization signals.

Our results indicate that the probability of detecting a polarization signal is approximately 0.016, corresponding to 16 events in our sample. These events are shown as orange dots in Figure 6. Using the bypass-transit limit $\bar{R}_h\ /u_0 \approx 0.75$ defined by Ingrosso et al., (2015), events with $(\bar{R}_h\ /u_0) > 0.75$ are classified as transit, while those with $(\bar{R}_h\ /u_0) < 0.75$ are classified as bypass. In our sample, we find 9 transit events and 7 bypass events. For transit events, the time interval between the peaks ranges nearly from 3 to 160 days. In bypass events, the duration during which the polarization signal remains above the detection threshold ranges from 7 to 45 days. These latter events are

particularly important, as finite-source effects are typically not detectable photometrically in such configurations.

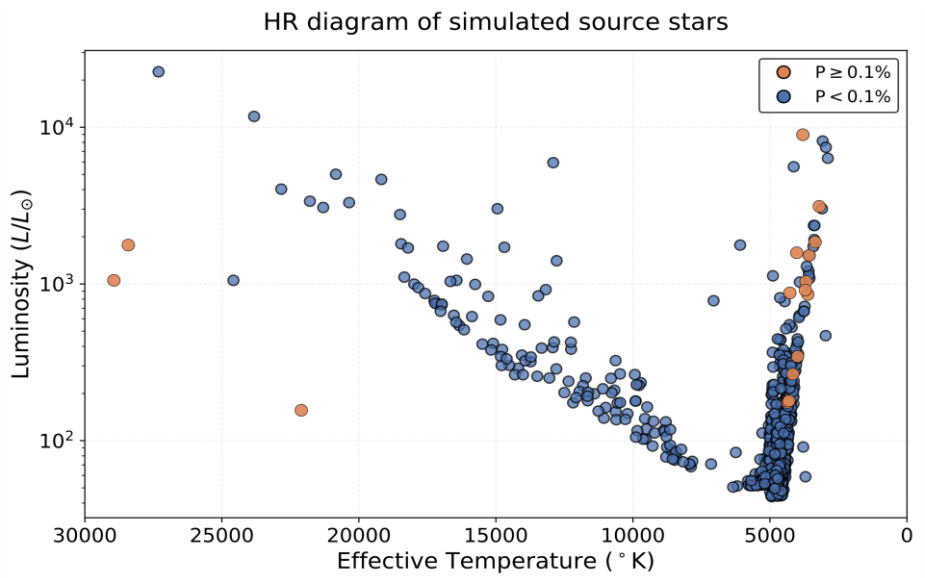

Figure 6: Scatter plot of 1000 simulated bulge stars showing their effective temperatures and luminosities. Orange points mark stars with possible detectable polarization signal, while blue points fall below the threshold.

Conclusions

Microlensing events offer a unique opportunity to probe compact dark objects, such as PBHs. Complementing this, polarimetric observations provide an additional method to refine lens parameters with greater precision. This study evaluates the detectability of polarization signals in PBH-induced microlensing events by combining observations from the Roman Space Telescope with polarimetric follow-up using the FORS2 instrument at the VLT.

Adopting the circumstellar envelope model of Simmons et al., (2002), our results indicate that compact lenses with masses in the range $10^{-3} - 10\ M_\odot$ are capable of producing polarization signals above the sensitivity threshold of FORS2 when located at distances up to 5 kpc from the observer along the line of sight toward the Galactic bulge. The polarization amplitude is found to

decrease for lenses located closer to the source, reflecting the reduced lensing efficiency at large lens distances.

Using source parameters generated via the IAC-STAR online tool, we estimate a detection probability of 1.6%. Among the detected polarized events, about 56% correspond to transit configurations, with time intervals between the peaks ranging from approximately 3 to 160 days. The remaining 44% of events are classified as bypass events, characterized by a single polarization peak that remains above the detection threshold for durations between roughly 7 and 45 days.

Finally, polarimetric observations of microlensing events observed by the Roman telescope have great potential to provide valuable insights that help break degeneracies inherent to photometric light curves alone. In addition, measuring the polarization angle will provide valuable information about the orientation of the lens trajectory during the event. Polarimetric data are particularly important in bypass events, where photometric observations alone are insufficient to determine the lensing parameters with certainty.

References

Alcock, C., Allsman, R. A., Alves, D., et al. (2000). The MACHO project: Microlensing results from 5.7 years of LMC observations. The Astrophysical Journal, 542(1), 281–307. https://doi.org/10.1086/309512

Bertelli, G., Bressan, A., Chiosi, C., Fagotto, F., & Nasi, E. (1994). Theoretical isochrones from models with new radiative opacities. Astronomy & Astrophysics Supplement Series, 106, 275–302.

Bond, I. A., Abe, F., Dodd, R. J., et al. (2001). Real-time difference imaging analysis of MOA Galactic bulge observations during 2000. Monthly Notices of the Royal Astronomical Society, 327(3), 868–880. https://doi.org/10.1046/j.1365-8711.2001.04776.x

Dominik, M. (2009). Parameter degeneracies and (un)predictability of gravitational microlensing events. Monthly Notices of the Royal Astronomical Society, 393(3), 816–826. https://doi.org/10.1111/j.1365-2966.2008.14276.x

Einstein, A. (1936). Lens-like action of a star by the deviation of light in the gravitational field. Science, 84(2188), 506–507. https://doi.org/10.1126/science.84.2188.506

Khalouei, E., Sajadian, S., & Rahvar, S. (2021). Measuring stellar atmosphere parameters using follow-up polarimetric microlensing observations. Monthly Notices of the Royal Astronomical Society, 501(3), 3203–3214. https://doi.org/10.1093/mnras/staa3492

Gaudi, B. S., Bennett, D. P., Udalski, A., et al. (2012). Discovery of a Jupiter/Saturn analog with gravitational microlensing. The Astrophysical Journal, 755(1), 42.

https://doi.org/10.1088/0004-637X/755/1/42

Green, A. M. (2017). Astrophysical uncertainties on stellar microlensing as a probe of primordial black hole dark matter. Physical Review D, 96(4), 043020.

https://doi.org/10.1103/PhysRevD.96.043020

Hafizi, M., De Paolis, F., Ingrosso, G., & Nucita, A. A. (2004). Microlensing signature of a white dwarf population in the Galactic halo. International Journal of Modern Physics D, 13(9), 1831–1845. https://doi.org/10.1142/S0218271804006036

Hamolli, L., De Paolis, F., Nucita, A. A., & Gashi, A. (2015). Finite source effects in microlensing by free-floating planets. International Journal of Modern Physics D, 24(07), 1550050.http://dx.doi.org/10.1155/2015/402303

Hamolli, L., Hafizi, M., Nucita, A. A., & De Paolis, F. (2019). Free-floating planets in the Milky Way. International Journal of Modern Physics D, 28(14), 1950167. https://doi.org/10.1007/s40065-019-0267-3

Hamolli, L., Hafizi, M., De Paolis, F., & Nucita, A. A. (2021). Gravitational microlensing constraints on primordial black holes by Euclid. arXiv preprint arXiv:2109.04857. https://arxiv.org/abs/2109.04857

Ingrosso, G., Calchi Novati, S., De Paolis, F., et al. (2012). Polarization in microlensing events towards the Galactic bulge. Monthly Notices of the Royal Astronomical Society, 426(2), 1496–1506. https://doi.org/10.1111/j.1365-2966.2012.21820.x

Ingrosso, G., De Paolis, F., Nucita, A. A., Strafella, F., Calchi Novati, S., Jetzer, P., Liuzzi, G., & Zakharov, A. (2014). Polarization in binary microlensing events. Physica Scripta, 89(8), 084001. https://doi.org/10.1088/0031-8949/89/8/084001

Ingrosso, G., Calchi Novati, S., De Paolis, F., Jetzer, P., Nucita, A. A., & Strafella, F. (2015). Measuring polarization in microlensing events. Monthly Notices of the Royal Astronomical Society, 446(1), 1090–1097. https://doi.org/10.1093/mnras/stu2161

Lejeune, T., Cuisinier, F., & Buser, R. (1997). Standard stellar library for evolutionary synthesis. Astronomy & Astrophysics Supplement Series, 125(2), 229–246.

Niikura, H., Takada, M., Yasuda, N., et al. (2019). Microlensing constraints on primordial black holes with Subaru/HSC Andromeda observations. Nature Astronomy, 3(6), 524–534. https://doi.org/10.1038/s41550-019-0723-1

Origlia, L., Ferraro, F. R., Fusi Pecci, F., & Rood, R. T. (2002). ISOCAM observations of Galactic globular clusters: Mass loss along the red giant branch. The Astrophysical Journal, 571(1), 458–472. https://doi.org/10.1086/339857

Paczyński, B. (1986). Gravitational microlensing by the galactic halo. The Astrophysical Journal, 304, 1–5. https://doi.org/10.1086/164140

Reimers, D. (1975). Circumstellar envelopes and mass loss of red giant stars. Memoires of the Societe Royale des Sciences de Liege, 8, 369–382.

Sajadian, S. (2023). Numerically studying the degeneracy problem in extreme finite-source microlensing events. Monthly Notices of the Royal Astronomical Society. https://doi.org/10.1093/mnras/stad945

Simmons, J. F. L., Newsam, A. M., & Willis, J. P. (1995a). Polarization in gravitational microlensing I: Theory and examples. Monthly Notices of the Royal Astronomical Society, 276(1), 182–200. https://doi.org/10.1093/mnras/276.1.182

Simmons, J. F. L., Willis, J. P., & Newsam, A. M. (1995). Polarisation as a tool for gravitational microlensing surveys. Astronomy & Astrophysics, 293, L46–L48.

Simmons, J. F. L., Bjorkman, J. E., Ignace, R., & Coleman, I. J. (2002). Polarization from microlensing of spherical circumstellar envelopes by a point lens. Monthly Notices of the Royal Astronomical Society, 336(2), 501–510.

https://doi.org/10.1046/j.1365-8711.2002.05766.x

Spergel, D., Gehrels, N., Breckinridge, J., et al. (2015). Wide-Field InfrarRed Survey Telescope-Astrophysics Focused Telescope Assets WFIRST-AFTA 2015 report. arXiv preprint. arXiv:1503.03757

Sumi, T., Kamiya, K., Bennett, D. P., et al. (2011). Unbound or distant planetary mass population detected by gravitational microlensing. Nature, 473(7347), 349–352. https://doi.org/10.1038/nature10092

Sureda, J., Magaˇna, J., Araya, I. J., Padilla, N. D. (2021) Press–schechter primordial blackhole mass functions and their observational constraints, Monthly Notices of the RoyalAstronomical Society 507, 4804.

Tinbergen, J. (2005). Astronomical polarimetry. Cambridge University Press.

Tisserand, P., Le Guillou, L., Afonso, C., et al. (2007). Limits on the Macho content of the Galactic halo from the EROS-2 survey of the Magellanic Clouds. Astronomy & Astrophysics, 469(2), 387–404. https://doi.org/10.1051/0004-6361:20066017

Wyrzykowski, Ł., Kozłowski, S., Skowron, J., et al. (2011). The OGLE view of microlensing towards the Magellanic Clouds. Monthly Notices of the Royal Astronomical Society, 413(1), 493–508. https://doi.org/10.1111/j.1365-2966.2010.18150.x